

# $D_1$ line broadening and hyperfine frequency shift coefficients for $^{87}\text{Rb}$ and $^{133}\text{Cs}$ in Ne, Ar, and $\text{N}_2$

Li-Chung Ha,\* Xianli Zhang, Nakri Dao, and K. Richard Overstreet  
 Frequency and Time Systems, Microchip, 34 Tozer Rd., Beverly, Massachusetts 01915, USA



(Received 24 November 2020; accepted 29 January 2021; published 19 February 2021)

Accurate measurements of optical line broadening and microwave hyperfine transition shifts are essential for optimizing the performance of buffer-gas atomic clocks. Previous literature has reported inconsistent measurement values. We report measurements of the  $D_1$  transition broadening and hyperfine frequency shift coefficients for  $^{87}\text{Rb}$  and  $^{133}\text{Cs}$  due to collisions with Ne and Ar atoms, as well as  $\text{N}_2$  molecules which is commonly employed for quenching in gas cell atomic clocks.

DOI: [10.1103/PhysRevA.103.022826](https://doi.org/10.1103/PhysRevA.103.022826)

## I. INTRODUCTION

Atomic clocks based on microwave double-resonance and coherent population trapping (CPT) are in common use today for their high stability and long-term timekeeping capabilities [1–3]. By far the most common atoms of choice are Rb and Cs for their low size, weight, power, and cost. The species of choice is often contained within a small, sealed glass cell for interrogation by lamp or laser light. In the absence of other gases, the atoms quickly lose phase coherence due to collisions with the cell wall, which leads to extreme broadening of the ground hyperfine transition and is detrimental to clock stability. To mitigate this effect, a mixture of other noble and inert molecular gases “buffer” the alkali-metal atom’s interaction with the cell wall [4]. Often, multiple gases are introduced to compensate for changes in temperature. The desired pressures of the buffer gases is a balance between mitigating wall collisions and minimizing broadening due to the buffer gas itself. Optimizing the buffer gas mixture requires accurate knowledge of the broadening and shift coefficients. Previous measurements of these shifts have reported inconsistent results [5–8]. While the reported coefficients have high precision, the uncertainty caused by the sample cell preparation is less discussed. In this work, we report on our sample preparation and experimental measurements, which we find to be in agreement with previous work. In addition, we also report direct measurements of  $^{87}\text{Rb}$  hyperfine frequency shift coefficients to second-order in temperature, beyond the linear model of prior studies. Having accurately calibrated coefficients is important for optimizing the performance of atomic clocks and even atomic sensors [9].

The collision shift is the primary contributor to the clock frequency shift of a gas cell atomic clock, orders of magnitude more than the light shift and the quadratic Zeeman shift. With a precise knowledge of gas composition, the buffer gas pressure can be calibrated by measuring the shift of the operating frequency of an atomic clock on the  $m_F = 0$  to  $m_F = 0$  ground-state hyperfine resonance. Bender *et al.* [7] first investigated the temperature dependence of  $^{87}\text{Rb}$  clock frequency

in Ar and  $\text{N}_2$ . Kozlova *et al.* [6] did a thorough investigation on the  $^{133}\text{Cs}$   $D_1$  line shift and the hyperfine frequency shift. The collisional shift coefficient can be modeled as [4]

$$\Delta\nu_{BG}/P = \frac{1}{\hbar k_B T} \int dE(r)_{HFS} e^{-U(r)/k_B T} r^2 dr, \quad (1)$$

where  $U(r)$  is the molecular potential between the buffer gas atoms and the alkali-metal atom, which is often simplified with a Lennard-Jones potential including an attractive  $1/r^6$  van der Waals attraction and a  $1/r^{12}$  short-range repulsive force.  $dE(r)_{HFS}$  is the perturbation on the hyperfine splitting from the buffer gas. The long-range attractive van der Waals force would result in a lower electron density at the core of the alkali atoms, therefore reducing the hyperfine splitting while the short-range repulsive force increases the splitting. A larger buffer gas atom or molecule could have a dominating van der Waals attraction and a negative shift coefficient [10]. The temperature dependence of the shift coefficient comes from the statistical weighing in the  $e^{-U(r)/k_B T}$  term. To second order, the temperature dependent shift for a sealed cell is

$$\Delta\nu = P_0[\beta + \delta(T - T_0) + \gamma(T - T_0)^2], \quad (2)$$

where  $P_0$  and  $T_0$  are the reference total pressure and temperature of the cell, and  $\beta$ ,  $\delta$  and  $\gamma$  are polynomial coefficients.  $\beta$ ,  $\delta$  and  $\gamma$  are characteristic of the temperature-dependent alkali-buffer gas interactions.

In addition to the collisional shift, the gas pressure may alternatively be measured by characterization of the optical absorption spectrum [11,12]. Both the spectral shift and broadening of the principal  $D_1$  and  $D_2$  transitions in Rb and Cs have been extensively characterized [13–21]. Wells *et al.* uses the isoclinic point of  $^{87}\text{Rb}$  to measure the  $D_1$  line shift with high precision [21]. The broadening measurement is generally more straightforward than the shift measurement because the sweep of the laser frequency may be directly calibrated from the spectrum by the ground hyperfine splitting. Most of those measurements are in agreement to within the error. However, the Cs broadening coefficient  $\Gamma$  in  $\text{N}_2$  has been controversial, and the reported values differ by almost a factor of two. The pressure uncertainty during the cell preparation is often not discussed, including the gas pressure change during the cell-sealing process. Furthermore, the temperature

\*Corresponding author: [lichung.ha@microchip.com](mailto:lichung.ha@microchip.com)

dependence also creates an additional barrier for direct comparison. The absorption broadening is mediated through the inelastic collisions with the background buffer gases, with the collision rate proportional to the gas density, collision cross section  $\sigma$ , and the gas velocity. Empirically, the broadening coefficient is normalized to the gas pressure with a specified measurement temperature. Occasionally, the broadening coefficient is normalized to the gas density. The latter method makes it convenient to measure the temperature dependence since a sealed cell has a constant density. Given a temperature-independent  $\sigma$ , the broadening coefficient scales with the temperature as

$$\Gamma_1 = \Gamma_2 (T_1/T_2)^n, \quad (3)$$

where  $n = 1/2$ . However, the prediction from the classical phase shift theory suggests that the exponent should scale as

$$n = \frac{p-3}{2(p-1)}, \quad (4)$$

where  $p$  is the exponent of the dominating molecular potential [22]. For buffer gases with a large van der Waals force,  $p = 6$  and  $n = 0.3$ . Kluttz *et al.* [15] measured a temperature-independent broadening exponent ( $n = 0.03 \pm 0.06$ ) for Rb  $D_1$  in  $N_2$ . It remains challenging to estimate the temperature dependence of the broadening coefficient, and more theoretical and experimental work is required.

## II. SAMPLE CELL PREPARATIONS

We prepare multiple sample resonance cells containing either  $^{133}\text{Cs}$  or  $^{87}\text{Rb}$  with varying pressures of Ne, Ar, or  $N_2$ . Cell pressure is calibrated with a mechanical manometer, which provides pressure measurements that are independent of gas type.

The resonance vapor cells are fabricated at the Microchip/FTS Beverly, MA facility. Empty cylindrical glass cells, measuring 22.4 mm length  $\times$  26.4 mm diameter are attached to a glassware manifold. The cells are loaded with either  $^{133}\text{Cs}$  or isotopically enriched  $^{87}\text{Rb}$  and then backfilled with one of the experimental gases. The gas pressures are calibrated at room temperature with mechanical manometers (Kurt J. Lesker, ACG-BT-1-1 for Cs and Edwards, Barocel pressure sensor for Rb). We estimate a potential systematic pressure error of less than 2% from the manometer. The cells are sealed and removed from the manifold utilizing a flame torch. The gas-density change due to the tipoff process is confirmed to be less than 1% by comparing the laser absorption spectrum before and after the seal at room temperature.

Each sample cell is inserted in an insulated metallic enclosure with a thermistor and heating resistors attached. The enclosure temperature is stabilized to a 0.1 °C precision with a commercial temperature controller (Omega, CNPT-Series). Because the cell temperature could deviate from the set temperature due to temperature gradients within the enclosure, an additional thermistor is used to measure the ambient temperature. We calibrate the ambient contribution in a commercial chamber (Associated Environmental Systems, BD-102). The temperature accuracy is better than 1 °C throughout the experiment.

## III. OPTICAL ABSORPTION MEASUREMENTS

The absorption spectrum of each sample was probed with a vertical-cavity surface-emitting laser (VCSEL). The VCSEL temperature was stabilized with an on-chip thermoelectric cooler (TEC). The VCSEL output frequency (wavelength) was controlled through variation of its bias current. The sweep of the current was slow enough (2 Hz) to produce a linear frequency scan. The maximum frequency nonlinearity is less than 2.2% of the scanning range measured with a wavelength meter (HighFinesse, WS-7-30). The laser power is kept at approximately 10  $\mu\text{W}$  throughout the measurements, and the laser intensity is far below (1%) the saturation intensity of the atomic transition to avoid power broadening. The laser polarization is tuned to  $\sigma+$  with a quarter-wave plate.

To extract the spectral data, we first process the absorption spectrum by subtracting the background from the raw signal. The transmission is calculated through normalizing the spectrum by scanning the laser frequency without the cell,

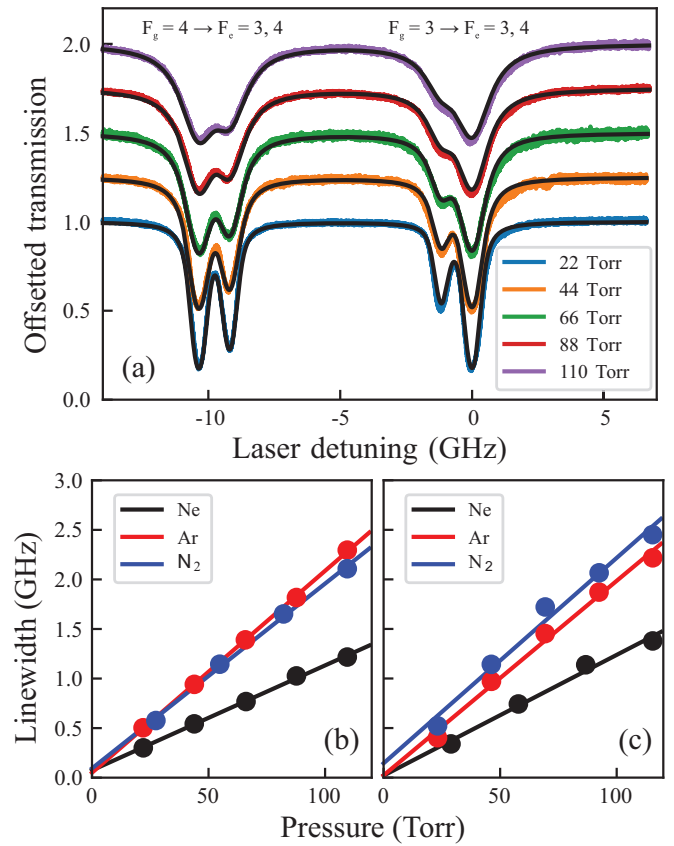


FIG. 1. Pressure broadening of the  $D_1$  line. (a) Cs absorption spectra in Ne buffer gas at different pressures. From low to high, the pressure is 22 torr (blue), 44 torr (orange), 66 torr (green), 88 torr (red), and 110 torr (purple). The black lines are the Voigt fit to the data. The transmission only accounts for the scattering from the atomic vapor and is normalized to 1 when the laser is far off-resonance. The spectra are offset (0.25 between curves) for visual clarity. Note that the laser intensity varies during the frequency scan, but the intensity slope is mathematically removed when calculating the transmission. (b), (c) Extracted Cs and Rb FWHM linewidths at different pressures for Ne (black), Ar (red), and  $N_2$  (blue). The error bars are smaller than the symbols.

TABLE I.  $D_1$  line broadening (FWHM) coefficients (left) and the collisional shift of the clock line (right) for Rb and Cs. We combine the statistical error and the potential 3% systematic error from the pressure calibration. Clock line shift coefficients are normalized to a reference pressure  $P_0$  at temperature  $T_0 = 0^\circ\text{C}$ . Note that the  $\gamma$  coefficients for  $^{87}\text{Rb}$  from [5] are scaled from the broad range measurement from  $^{85}\text{Rb}$  [24].

	T (K)	$\Gamma$ (MHz/torr)	Ref.	$\beta$ (Hz/torr)	$\delta$ (Hz/torr K)	$\gamma$ (mHz/torr K <sup>2</sup> )	Ref.
Cs/Ne	320	$10.6 \pm 0.41$	This work	$604.3 \pm 19.7$	$0.25 \pm 0.04$	$-1.72 \pm 0.48$	This work
	313	$10.85 \pm 0.02$	[19]	$686 \pm 14$	$0.266 \pm 0.006$	$-1.68 \pm 0.05$	[6]
	295	$10.13 \pm 0.86$	[20]				
Cs/Ar	320	$20.4 \pm 0.65$	This work	$-182.2 \pm 5.5$	$-1.12 \pm 0.05$	$-0.40 \pm 0.43$	This work
	295	$19.64 \pm 0.23$	[20]	$-194.4 \pm 1.6$	$-1.138 \pm 0.010$	$0.0 \pm 0.3$	[6]
	313	$18.31 \pm 0.16$	[19]	$-191.4 \pm 3.0$	$-1.05 \pm 0.05$		[8]
Cs/N <sub>2</sub>	320	$18.6 \pm 0.85$	This work	$879.3 \pm 26.6$	$0.89 \pm 0.11$	$-3.22 \pm 1.28$	This work
	294	$19.51 \pm 0.06$	[17]	$922.5 \pm 4.8$	$0.824 \pm 0.006$	$-2.51 \pm 0.03$	[6]
	393	$14.73 \pm 0.69$	[18]	$924.7 \pm 7.0$	$0.623 \pm 0.050$		[8]
	318	$15.82 \pm 0.05$	[19]				
	295	$30.93 \pm 5.71$	[20]				
Rb/Ne	337	$12.2 \pm 0.97$	This work	$423.1 \pm 12.7$	$0.35 \pm 0.05$	$-1.10 \pm 0.50$	This work
	320	$9.4 \pm 1.3$	[13]	$414 \pm 9$	$0.28$		[7]
	394	$9.84 \pm 0.1$	[14]				
Rb/Ar	337	$19.6 \pm 1.2$	This work	$-48.4 \pm 1.5$	$-0.29 \pm 0.07$	$-0.80 \pm 0.65$	This work
	320	$18.2 \pm 2.4$	[13]	$-50.96$	$-0.34$	$-0.4$	[5]
	394	$18.1 \pm 0.2$	[14]	$-48 \pm 1$	$-0.32$		[7]
Rb/N <sub>2</sub>	337	$20.4 \pm 1.4$	This work	$553.1 \pm 16.6$	$0.84 \pm 0.06$	$-1.77 \pm 0.45$	This work
	394	$16.3 \pm 0.4$	[14]	$624.33$	$0.82$	$-1.58$	[5]
	353	$17.73 \pm 0.13$	[15]	$544 \pm 11$	$0.64$		[7]
	353	$18.12 \pm 0.31$	[16]				

which has a linear intensity slope with respect to the forward current given by the slope efficiency and the lasing threshold of the VCSEL. We then scale the far off-resonant transmission to 1, which removes the contribution from the cell reflection and Cs coating on the windows [see Fig. 1(a)]. The Lorentzian width and the resonance optical density ( $c$ ) of each sample cell are extracted by fitting each laser absorption spectrum to a model spectrum ( $e^{-c\sum a_i V_i}$ ) comprised of four Voigt functions ( $V_i$ ). The four Voigt functions are fit by assuming equal linewidth. Note that a Voigt function is the convolution between a Lorentzian function of the atomic transition and a Gaussian function due to Doppler broadening. The Doppler contribution to the line broadening, spacing of the resonance lines, and the relative line strengths ( $a_i$ ) are fixed. The Doppler widths at our operating temperature for Cs (320.0 K) and Rb (337.3 K) are 370 and 530 MHz, respectively. The line spacing is scaled to the hyperfine splittings. Despite the perturbation from the collisional shift, we estimate the systematic error due to ignoring the collisional shift to be smaller than  $1 \times 10^{-5}$  within our pressure range. The relative line strengths are calculated through summing up the contributions from all dipole matrix elements from states with various projected angular momenta, which is only valid for low laser intensity.

The extracted full width at half maximum (FWHM) linewidths at different cell pressures are shown in Figs. 1(b) and 1(c). The pressure is projected from the sealing temperature ( $19^\circ\text{C}$ ) to the measurement temperatures with the ideal-gas law. The uncertainty of the Cs linewidth is significantly smaller when compared with the Rb measurement due to its larger hyperfine splitting. Our VCSEL linewidth is approximately 30 MHz, which is not negligible in the

absorption linewidth broadening measurement. However, by measuring the broadened width at multiple pressures, we remove the contribution from the laser linewidth in the analysis. The y-axis intercept corresponds to the convolution of the natural linewidth with the laser linewidth, and the slope is the broadening coefficient.

Our primary systematic error is the pressure calibration, which is 3%. Power broadening only contributes an error of 25 kHz which is five orders of magnitude smaller than our interested range. Contribution from the relaxation due to wall collision is less than 10 kHz.

The extracted broadening coefficients are presented in the second column of Table I. Our results are in reasonable agreement with most of the literature numbers except for the Cs  $\Gamma$  coefficient in N<sub>2</sub>. This broadening coefficient reported by Bernabeu *et al.* [20] has a large uncertainty and is significantly different from recent measurements. Andalkar *et al.* [17] revisited the measurement and have done a thorough investigation to reduce all possible errors. Couture *et al.* [18] reported an even lower number, which may be the consequence of their high measurement temperature. We do not know the reason for the discrepancy with Pitz *et al.* [19] in the Ar and N<sub>2</sub> measurements.

Our Rb broadening measurements are systematically larger than other references. This could be caused by the merging of spectral lines at a high pressure. The fitting routine has fewer features to constrain the linewidth estimation at the lower bound. This is limited by the smaller hyperfine splitting of Rb atoms. The uncertainty is reflected in the larger error bar. The extrapolation to zero-pressure linewidth is particularly worse for N<sub>2</sub> due to its large broadening coefficient.

In regimes where the transitional wavelength is much larger than the mean-free path, the Dicke effect [23] can cause line narrowing through modification of the gas velocity distribution, which may introduce systematic errors in the Voigt fitting. These errors are small enough to be ignored in our broadening coefficient measurements but could be exacerbated in the temperature-dependence measurements, specifically by imposing an unknown effective Doppler width in the Voigt profile. Hence, we compare our measured coefficients with various references without applying any temperature scaling and only list the measurement temperatures in Table I. Note that the large discrepancy in the Rb broadening coefficient measurements between Rotondaro and Perram [14] and this work could be the consequence of the temperature dependence.

#### IV. HYPERFINE FREQUENCY SHIFT MEASUREMENTS

The clock frequency shift was measured with CPT spectroscopy [25,26]. When illuminating the alkali vapor with two laser beams, transmission of the total power can increase when the frequency difference matches the ground hyperfine splitting. A fraction of the alkali atoms are trapped in the coherent superposition of the two ground states and do not contribute to the scattering. A convenient way to have two laser frequency components is to generate sidebands by direct modulation of the laser bias current. Compared with the optical-microwave double-resonance spectroscopy, CPT spectroscopy avoids systematic errors due to cavity pulling. We coupled a microwave source at one-half of the ground-state hyperfine frequency to the laser bias current. The microwave frequency was referenced to the Microchip/FTS house frequency standard, which contributes an error of  $8 \times 10^{-14}$  to the measurements. The microwave power was tuned to maximize the absorption signal from the first sidebands at half the clock frequency. The laser current was stabilized at the center of  $D_1$  transitions with the absorption signal by using a lock-in amplifier (Zurich Instruments, HF2LI). Figure 2(a) shows the CPT spectrum of Rb vapor cells containing Ar buffer gas at five different pressures. We measure the displacement of the CPT resonance peak with an open-loop microwave frequency scan and extract the pressure shift. The statistical uncertainty of the frequency shift is smaller than 5 Hz. Figures 2(b) and 2(c) are the pressure shifts of Cs and Rb, respectively, for three different buffer gases. While Ne and  $N_2$  have positive pressure shifts, Ar shows a negative trend.

We measured the hyperfine clock frequency shift coefficients,  $\beta$ ,  $\delta$ , and  $\gamma$ , on the 100 torr (at fill) cells [see Figs. 3(a) and 3(b)] and fit the measurement over the range between 30 and 65 °C with Eq. (2). The pressure  $P_0$  is scaled to a reference temperature of  $T_0 = 0$  °C. The extracted coefficients are presented on the right-hand side of Table I. Our results agree with most reported values within the statistical error and the potential 3% systematic error in our cell pressure. The results from Vanier *et al.* [5] and Bender *et al.* [7] are scaled to our  $T_0$ . Note that we estimate the light shift to be around a few Hz at our laser intensity and microwave power. Although the light shift can change with the cell temperature due to the varying optical density, the contribution to the error of the temperature coefficients is negligible.

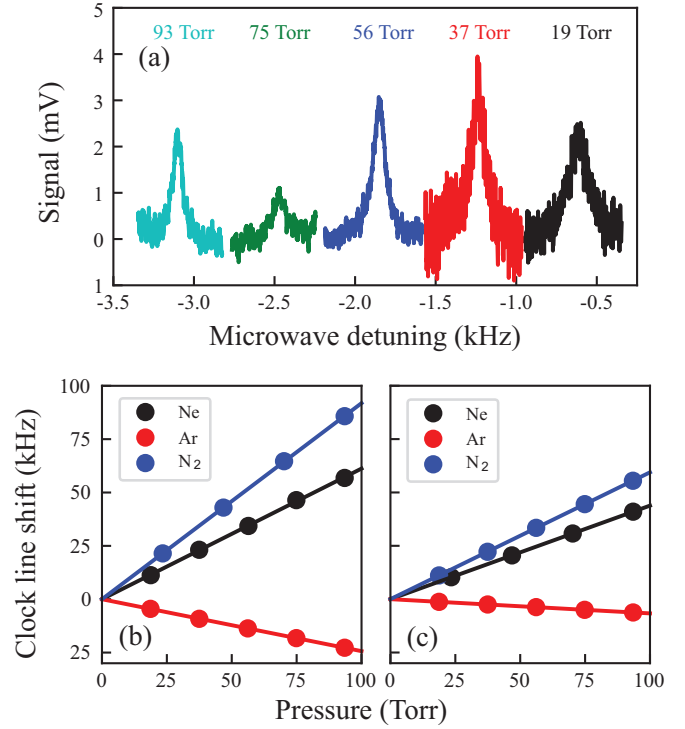


FIG. 2. Pressure shift of the clock transition. (a) CPT spectra for Rb with Ar buffer gas at different pressures, including 19 torr (black), 37 torr (red), 56 torr (blue), 75 torr (green), and 93 torr (cyan). The CPT FWHM linewidth reduces from 192 to 90 Hz when the buffer gas pressure increases, indicating mitigation of wall collision relaxation. The lower signal strength of the 75-torr data is caused by laser attenuation due to Cs coating on the cell windows. (b), (c) Linear fit of the extracted Cs and Rb clock line shift at different pressures of Ne (black), Ar (red), and nitrogen (blue). The pressure is scaled to the 0 °C pressure based on the ideal-gas law.

This is a direct measurement of  $\gamma$  for  $^{87}\text{Rb}$  in the gases of interest. CPT spectroscopy provides a more precise method to extract the quadratic temperature dependence in a small temperature range. The  $\gamma$  coefficients reported by Vanier *et al.* [5] were transformed from the broad range measurements of

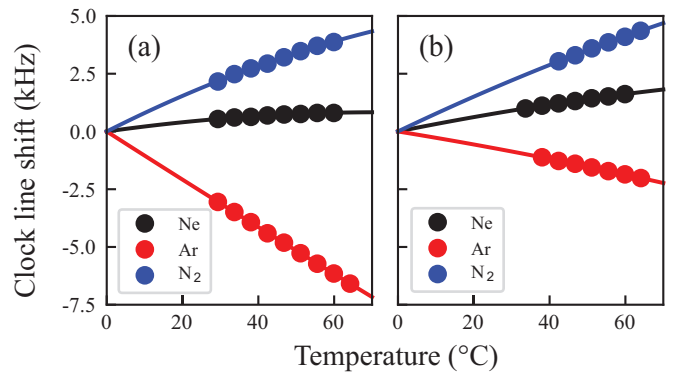


FIG. 3. Temperature shift. Temperature dependence of the clock line shift for both the (a) Cs and (b) Rb. All measurements are done with the 100 torr cells. The symbols are Ne (black), Ar (red), and nitrogen (blue).



<sup>85</sup>Rb made by Bean and Lambert [24] by multiplying the coefficients by the ratio of the hyperfine frequencies.

Our measurements agree with most of the literature. The Cs  $\beta$  coefficient in Ne, however, is significantly different from that of Kozlova *et al.* [6], while  $\delta$  and  $\gamma$  are consistent. Our  $\beta$  coefficient is based on the derivative of the collisional shift with respect to the pressure, which is immune to the common-mode bias when measuring the shift at few specific pressures. We found similar inconsistencies when comparing our Rb  $\beta$  coefficient in N<sub>2</sub> with the result from Vanier *et al.* [5].

## V. CONCLUSIONS

We have performed independent measurements of the  $D_1$  transition broadening and the hyperfine frequency shift for both <sup>133</sup>Cs and <sup>87</sup>Rb. Our results provide a consistent pressure characterization with two independent methods, therefore, the measured coefficients are more likely to be accurate

when compared with prior publications. This is important for designing the next-generation gas cell atomic sensors [9] and providing a better manufacturing quality control in the existing atomic clock products. We also present a CPT measurement for the clock line shift and a direct measurement of  $\gamma$  coefficients for <sup>87</sup>Rb in Ne, Ar, and N<sub>2</sub>. While the the gas cell atomic clock was invented more than 60 years ago, the continuous technology innovation, including chip-scale atomic clocks, demands a better and more accurate understanding of the individual components.

## ACKNOWLEDGMENTS

This work benefited greatly from the support of the Microchip/FTS manufacturing team. We thank Armando Martins, Paul Kiricoples, and Matthew McDonald for manufacturing the Cs cells, and Amy Mariano and Emmett Pierro for manufacturing the Rb cells. We also thank Robert Lutwak for carefully reading the manuscript.

- 
- [1] W. J. Riley, *Rubidium Frequency Standard Primer* (Hamilton Technical Services, Beaufort, SC, 2011).
  - [2] S. Knappe, V. Shah, P. D. D. Schwindt, L. Hollberg, J. Kitching, L.-A. Liew, and J. Moreland, A microfabricated atomic clock, *Appl. Phys. Lett.* **85**, 1460 (2004).
  - [3] R. Lutwak, P. Vlitaz, M. Varghese, M. Mescher, D. K. Serkland, and G. M. Peake, The Mac - a Miniature Atomic Clock, *Proceedings of the IEEE International Frequency Control Symposium and Exposition, Vancouver* (IEEE, Vancouver, BC, Canada, 2005), p. 752.
  - [4] J. Vanier and C. Audoin, *The Quantum Physics of Atomic Frequency Standards* (Adam Hilger, Philadelphia, 1989).
  - [5] J. Vanier, R. Kunski, N. Cyr, J. Y. Savard, and M. Têtu, On hyperfine frequency shifts caused by buffer gases: Application to the optically pumped passive rubidium frequency standard, *J. Appl. Phys.* **53**, 5387 (1982).
  - [6] O. Kozlova, S. Guérandel, and E. de Clercq, Temperature and pressure shift of the Cs clock transition in the presence of buffer gases: Ne, N<sub>2</sub>, Ar, *Phys. Rev. A* **83**, 062714 (2011).
  - [7] P. L. Bender, E. C. Beaty, and A. R. Chi, Optical Detection of Narrow Rb<sup>87</sup> Hyperfine Absorption Lines, *Phys. Rev. Lett.* **1**, 311 (1958).
  - [8] F. Strumia, N. Beverini, A. Moretti, and G. Rovera, Optimization of the buffer gas mixture for optically pumped Cs frequency standard, *Proceedings of the 30th Annual Symposium Frequency Control* (IEEE, Atlantic City, NJ, USA, 1976), p. 468.
  - [9] J. Kitching, Chip-scale atomic devices, *Appl. Phys. Rev.* **5**, 031302 (2018).
  - [10] M. Arditi and T. R. Carver, Frequency shift of the zero-field hyperfine splitting of Cs<sup>133</sup> produced by various buffer gases, *Phys. Rev.* **112**, 449 (1958).
  - [11] W. R. Hindmarsh and J. M. Farr, Collision broadening of spectral lines by neutral atoms, *Prog. Quantum Electron.* **2**, 141 (1973).
  - [12] N. Allard and J. Kielkopf, The effect of neutral nonresonant collisions on atomic spectral lines, *Rev. Mod. Phys.* **54**, 1103 (1982).
  - [13] C. Ottinger, R. Scheps, G. W. York, and A. Gallagher, Broadening of the Rb resonance lines by the noble gases, *Phys. Rev. A* **11**, 1815 (1975).
  - [14] M. D. Rotondaro and G. P. Perram, Collisional broadening and shift of the rubidium  $D_1$  and  $D_2$  lines ( $5^2S_{1/2} \rightarrow 5^2P_{1/2}, 5^2P_{3/2}$ ) by rare gases, H<sub>2</sub>, D<sub>2</sub>, N<sub>2</sub>, CH<sub>4</sub> and CF<sub>4</sub>, *J. Quant. Spectrosc. Radiat. Transfer* **57**, 497 (1997).
  - [15] K. A. Klutetz, T. D. Averett, and B. A. Wolin, Pressure broadening and frequency shift of the  $D_1$  and  $D_2$  lines of Rb and K in the presence of He and N<sub>2</sub>, *Phys. Rev. A* **87**, 032516 (2013).
  - [16] M. V. Romalis, E. Miron, and G. D. Cates, Pressure broadening of Rb  $D_1$  and  $D_2$  lines by <sup>3</sup>He, <sup>4</sup>He, N<sub>2</sub>, and Xe: Line cores and near wings, *Phys. Rev. A* **56**, 4569 (1997).
  - [17] A. Andalkar and R. B. Warrington, High-resolution measurement of the pressure broadening and shift of the Cs  $D_1$  and  $D_2$  lines by N<sub>2</sub> and He buffer gases, *Phys. Rev. A* **65**, 032708 (2002).
  - [18] A. H. Couture, T. B. Clegg, and B. Driehuys, Pressure shifts and broadening of the Cs  $D_1$  and  $D_2$  lines by He, N<sub>2</sub>, and Xe at densities used for optical pumping and spin exchange polarization, *J. Appl. Phys.* **104**, 094912 (2008).
  - [19] G. A. Pitz, D. E. Wertepny, and G. P. Perram, Pressure broadening and shift of the cesium  $D_1$  transition by the noble gases and N<sub>2</sub>, H<sub>2</sub>, HD, D<sub>2</sub>, CH<sub>4</sub>, C<sub>2</sub>H<sub>6</sub>, CF<sub>4</sub>, and <sup>3</sup>He, *Phys. Rev. A* **80**, 062718 (2009).
  - [20] E. Bernabeu and J. M. Alvarez, Shift and broadening of hyperfine components of the first doublet of cesium perturbed by foreign gases, *Phys. Rev. A* **22**, 2690 (1980).
  - [21] N. P. Wells, T. U. Driskell, and J. C. Camparo, Fine-structure mixing in Rb-Xe elastic collisions and isoclinic point asymmetry, *Phys. Rev. A* **92**, 022505 (2015).
  - [22] A. Bielski, R. Bobkowski, and J. Szudy, Power-law dependence of the pressure broadening of spectral lines on temperature, *Astron. Astrophys.* **208**, 357 (1989).

- [23] R. H. Dicke, The effect of collisions upon the Doppler width of spectral lines, [Phys. Rev. \*\*89\*\*, 472 \(1953\)](#).
- [24] B. L. Bean and R. H. Lambert, Temperature dependence of hyperfine density shifts. IV.  $^{23}\text{Na}$ ,  $^{39}\text{K}$ , and  $^{85}\text{Rb}$  in He, Ne, Ar, and  $\text{N}_2$  at low temperatures, [Phys. Rev. A \*\*13\*\*, 492 \(1976\)](#).
- [25] E. Arimondo and G. Orriols, Nonabsorbing atomic coherences by coherent two-photon transitions in a three-level optical pumping, [Lett. Nuovo Cimento \*\*17\*\*, 333 \(1976\)](#).
- [26] R. M. Whitley and C. R. Stroud, Double optical resonance, [Phys. Rev. A \*\*14\*\*, 1498 \(1976\)](#).